The two-loop method for determination of dynamic stress intensity factors from dynamic isochromatic crack-tip stress patterns

H. P. ROSSMANITH (VIENNA)

THE STATIC three-parameter method as developed by Dally and Etheridge for the determination of stress intensity factors from data pertaining to a pair of non-identical isochromatic crack-tip fringe loops is generalized to the dynamic case. The influence of the transition from plane strain to plane stress when selecting larger loops is discussed. Generalized stress intensity factor versus fringe loop tilt angle relationships and various adjustments are presented, which include both dynamic and higher order term corrections.

Statystyczną metodę trójparametrową rozwiniętą przez Dally'ego i Etheridge'a służącą do określania współczynników intensywności naprężenia na podstawie danych dotyczących pary nieidentycznych pętli izochrom w wierzchołku szczeliny uogólniono w niniejszej pracy na przypadek dynamiczny. Przedyskutowano wpływ przejścia z płaskiego stanu odkształcenia do płaskiego stanu naprężenia przy wyborze coraz większych pętli. Przedstawiono zależność między uogólnionym współczynnikiem intensywności naprężenia a kątem nachylenia pętli oraz omówiono różne człony korekcyjne wynikające z efektów dynamicznych i poprawek wyższego rzędu.

Статический трехпараметрический метод, развитый Далли и Этериджом и служащий для определения коэффициентов интенсивности напряжений на основе данных, касающихся пары неидентичных петлей изохром в вершине щели, обобщен в настоящей работе на динамический случай. Обсуждено влияние перехода из плоского деформационного состояния в плоское напряженное состояние, при выборе все больших петлей. Представлена зависимость между обобщенным коэффициентом интенсивности напряжений и углом наклона петли, а также обсуждены разные поправочные члены, вытекающие из динамических поправок и поправок высшего порядка.

1. Introduction

A COMMON procedure for the determination of the stress intensity factor K from photoelastic data was introduced by IRWIN in 1958 [1]. In this method, the stress around a crack tip can be characterized by two parameters, the intensity factor K, and a uniform stress σ_{0x}, and may be evaluated from measurements of the apogee distance r_m, of a fringe loop and the fringe loop tilt angle θ_m (Fig. 1).

Since then, BRADLEY and KOBAYASHI [2] have modified Irwin's method employing a technique which involves measurements of r_m and θ_m on two different fringe loops.

ETHERIDGE et al. [3] introduced an additional parameter β into the analysis to account for finite boundary effects. This two-term truncation of the Taylor series expansion of the "Westergaard" stress function allows the use of larger isochromatic fringe loops which exceed the range of applicability of the singular stress field analysis. A static two-loop method has been developed by ETHERIDGE and DALLY [4] where a cubic equation for β was derived.

All the preceding methods of analysis pertain to the static case. Recently, ROSSMANITH and IRWIN [5] generalized the methods to the dynamic case. Here, a dynamic two-loop method is developed and a simple cubic equation for β is presented.
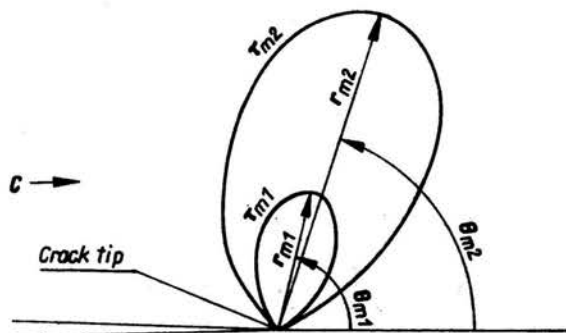
FIG. 1. Characteristic geometry of a pair of isochromatic fringe loops at the crack tip.

2. Analysis

The dynamic stress field around a running opening mode crack can be represented by [6]

$$
\begin{aligned}
\sigma_x &= A\mu\{(2r_1^2 - r_2^2 - 1)\operatorname{Re} Z_1 - \Omega \operatorname{Re} Z_2\} + \sigma_{0x}, \\
\sigma_y &= A\mu\{-(1 + r_2^2)\operatorname{Re} Z_1 + \Omega \operatorname{Re} Z_2\}, \\
\tau_{xy} &= A\mu 2r_1 \{\operatorname{Im} Z_2 - \operatorname{Im} Z_1\},
\end{aligned}
\tag{1}
$$

where Re and Im denote the real and imaginary parts of the complex two-term Westergaard type stress function

$$
Z_j = \frac{K}{\sqrt{2\pi z_j}}\left[1 + \beta\frac{z_j}{a}\right].
\tag{2}
$$

The coefficient A may be determined from the boundary conditions and is given by

$$
A\mu = \frac{1 + r_2^2}{4r_1 r_2 - (1 + r_2^2)^2},
\tag{3}
$$

where μ is the shear modulus, $r_j^2 = 1 - (c/c_j)^2$ $(j = 1, 2)$; c is the crack tip speed, c_1 and c_2 are the longitudinal and transversal wave velocities, respectively, for plane waves in an infinite medium and $\Omega = 4r_1 r_2/(1 + r_2^2)$. Figure 2 provides some advantageous geometrical relationships between z_j and z:

$$
\begin{aligned}
z &= x + iy = re^{i\theta}, \\
z_j &= x + iy_j = \varrho_j e^{i\theta_j},
\end{aligned}
\tag{4}
$$

$$
\varrho_j = r\sqrt{1 - (c/c_j)^2\sin^2\theta} \equiv r\gamma_j^2,
\tag{5}
$$

$$
\tan\theta_j = r_j\tan\theta \quad (j = 1, 2).
\tag{6}
$$
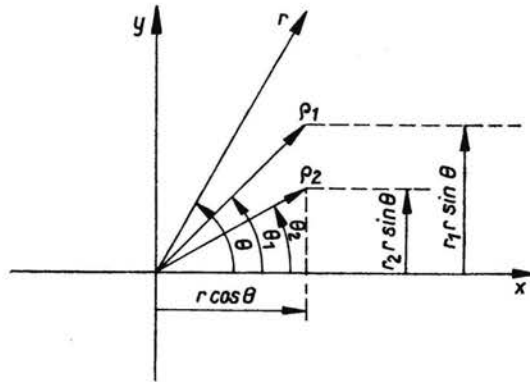
FIG. 2. Crack tip coordinate systems employed in the stress function analysis.

Employing the relations (4)—(6), the real and imaginary parts of the stress functions (2) take the form

$$(7) \qquad \mathrm{Re}\, Z_j(z) = \frac{K}{\sqrt{2\pi r}} \frac{1}{\gamma_j} \cos\frac{\theta_j^{\cdot}}{2}\left(1+\beta\frac{r}{a}\gamma_j^2\right),$$

$$(8) \qquad \mathrm{Im}\, Z_j(z) = -\frac{K}{\sqrt{2\pi r}} \frac{1}{\gamma_j} \sin\frac{\theta_j}{2}\left(1-\beta\frac{r}{a}\gamma_j^2\right),$$

and upon substitution into Eqs. (1), the stresses take the form

$$\sigma_x = \frac{A\mu K}{\sqrt{2\pi r_s}}\sqrt{\frac{r_s}{r}}\left\{(2r_1^2-r_2^2+1)C_c^1\left(1+\beta\frac{r}{r_s}\gamma_1^2\right)-\Omega C_c^2\left(1+\beta\frac{r}{r_s}\gamma_2^2\right)+\frac{\alpha^*}{A\mu}\right\},$$

$$(9) \qquad \sigma_y = \frac{A\mu K}{\sqrt{2\pi r_s}}\sqrt{\frac{r_s}{r}}\left\{-(1+r_2^2)C_c^1\left(1+\beta\frac{r}{r_s}\gamma_1^2\right)+\Omega C_c^2\left(1+\beta\frac{r}{r_s}\gamma_2^2\right)\right\},$$

$$\tau_{xy} = \frac{A\mu K}{\sqrt{2\pi r_s}}\sqrt{\frac{r_s}{r}}\,2r_1\left\{C_s^1\left(1-\beta\frac{r}{r_s}\gamma_1^2\right)-C_s^2\left(1-\beta\frac{r}{r_s}\gamma_2^2\right)\right\},$$

where the abbreviations C_s^j, C_c^j $(j=1,2)$ are given in the Appendix and the parameter α involving σ_{0x} is given by

$$(10) \qquad \alpha = \frac{\sigma_{0x}\sqrt{2\pi r_s}}{K}, \qquad \alpha^* = \alpha\sqrt{\frac{r}{r_s}}$$

and controls the character of the biaxial stress field near the crack tip.

The maximum in-plane shear stress is

$$(11) \qquad (2\tau_m)^2 = (\sigma_y-\sigma_x)^2+(2\tau_{xy})^2.$$

From the fringe loop geometry, it follows that

$$(12) \qquad \frac{\partial\tau_m}{\partial\theta}\bigg|_{\substack{\theta=\theta_m\\ r=r_m}} = 0,$$

where r_m is the apogee distance and θ_m is the associated fringe loop tilt angle.

Substituting Eqs. (9) into Eq. (11) and employing Eq. (12) gives an equation

$$(13) \qquad \frac{\sigma_{0x}\sqrt{2\pi r_{mj}}}{K} \equiv \alpha\sqrt{\frac{r_{mj}}{r_s}} = -(F+Gg)_{\substack{\theta=\theta_{jm} \\ r=r_{jm}}} = \chi(\theta_{mj}, r_{mj}, \beta),$$

which holds for each fringe loop. Since σ_{0x} and K do not depend on the orders of the fringe loops, the transition from one loop to another loop $r_{mi} \to r_{mj}$, $\theta_{mi} \to \theta_{mj}$ changes only the value of β. This is obvious since loops of different sizes are differently influenced by the specimen boundaries. The radius r_s in Eq. (13) is a reference radius. It is usually chosen to equal the radius of the region of applicability of the near crack tip analysis. The quantities F, G and g are given in the Appendix. By selecting two non-identical loops ($i \equiv 1$ and $j \equiv 2$) and equating their associated expressions (13)

$$(14) \qquad \sqrt{\frac{r_{m1}}{r_{m2}}}\{F_2+G_2g_2\} = F_1+G_1g_1$$

a cubic equation for β may be derived

$$(15) \qquad \beta^3(\lambda_6-\xi\lambda_{12})+\beta^2(\lambda_4-\lambda_{10}-\lambda_{11}\xi^2+\lambda_5\xi^{-2})$$
$$+\beta(-\lambda_9\xi^{-1}+\lambda_2-\lambda_8\xi+\lambda_3\xi^2)+\lambda_1\xi-\lambda_7 = 0,$$

where $\xi = \sqrt{r_{m1}/r_{m2}}$ and the expressions for λ_k and F_j, G_j and g_j ($j = 1, 2$) are given in the Appendix. The arbitrary reference radius r_s has been selected to equal the square root of r_{m1} times r_{m2}.

The solution of Eq. (15) yields three values for

$$(16) \qquad \beta_l = \beta_l(\theta_{m1}, \theta_{m2}, r_{m1}, r_{m2}); \quad (l = 1, 2, 3),$$

which are substituted into Eq. (13) to obtain three values of α. These three solution pairs are then substituted into Eq. (11) to obtain three values of the stress intensity factor K. It is obvious for physical reasons that only the solution for β which provides real-valued positive K-values is of practical interest. The value of α may be negative (SEN-specimen, $\theta_m < 90°$) or positive (CT-specimen, $90° < \theta_m < 110°$; DCB-specimen, $110° < \theta_m < 145°$). The magnitude and sign of the β-term are controlled by the fracture test specimen geometry and loading conditions, and change during crack propagation [5].

By combining Eqs. (9), (11) and (13) one obtains

$$(17) \qquad \frac{K}{2\tau_m\sqrt{2\pi r_m}} = H(\theta_m, r_m, \beta) \equiv \frac{1}{G\sqrt{1+g^2}},$$

where $H(\theta_m, r_m, \beta)$ is a function of θ_m, r_m and β. The expressions for G and $\dot{g}$ are given in the Appendix.

The appropriate value of β from Eq. (16) is substituted into Eq. (17) to yield an expression for the stress intensity factor K in terms of the six parameters θ_m, r_m, θ_{m1}, r_{m1}, θ_{m2}, and r_{m2}. It is convenient to let two pairs of parameters coincide (e.g. $\theta_m \equiv \theta_{m1}$, $r_m \equiv r_{m1}$). This gives the fundamental relationship for the dynamic two-loop method.

$$(18) \qquad K_n \equiv \frac{K}{2\tau_m\sqrt{2\pi r_{m1}}} = H(\theta_{m1}, r_{m1}; \theta_{m2}, r_{m2}),$$

where K_n is a normalized stress intensity factor.

Discussion

The β term is a time-dependent function for a propagating crack. The magnitude and sign of $\beta(t)$ depend primarily on the geometry of the fracture test specimen and the load conditions, i.e. β depends on the dynamics of the test specimen. For almost all cases, β is expected to increase monotonically when the crack propagates under „fixed grip" conditions.

It should be noted that any given combination of two fringe loops of different order will give a β-value somewhat different from that given by any other combination. Thus the solution (16) as well as the K-value derived depend on the loops selected.

The following β-dependent K vs θ_m study covers a wide range of β values. The influence of the β term on the K vs θ_m curve is appreciable. Figures 3a and 3b show that the range of the K_n vs θ_m relationship is a function of the sign and magnitude of β, and that corresponding dynamic K values (Fig. 3b) are smaller than the static-values (Fig. 3a). For the static two-parameter method ($\beta = 0$), the range of validity of the K vs θ_m relationship is limited by the two singularities at $\theta_m = 69.5°$ and $\theta_m = 148.5°$. Increasing positive (decreasing negative) β-values shift this range to the left (right) when the singularities move towards lower (higher) θ_m-angles. Figure 4 compares the adjustment or relative error, $E_{\beta\beta}^{sd}$, in percent which is introduced if one employs the static three-parameter method rather than the dynamic three-parameter method for K-determination. The minimum adjustment is 11% for $\theta_m = 105°$ in the case of a high speed running crack ($c = 16000''/s$). The adjustment of relative error $E_{\beta\beta}^{sd}$ increases when the tilt angle becomes larger or smaller than $\theta_m = 105°$. This is the case for SEN-specimens, where the fringe loops lean forward ($\theta_m < 90°$) and for DCB specimens, where the loops tilt strongly backward ($\theta_m \gtrsim 130°$). Finally, Fig. 5 compares the adjustment or relative error $E_{0\beta}^{ds}$ in percent which is made
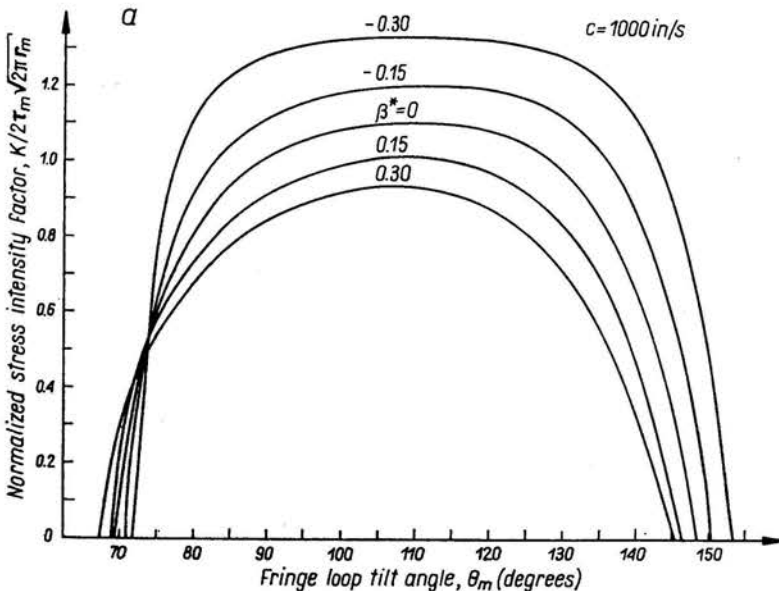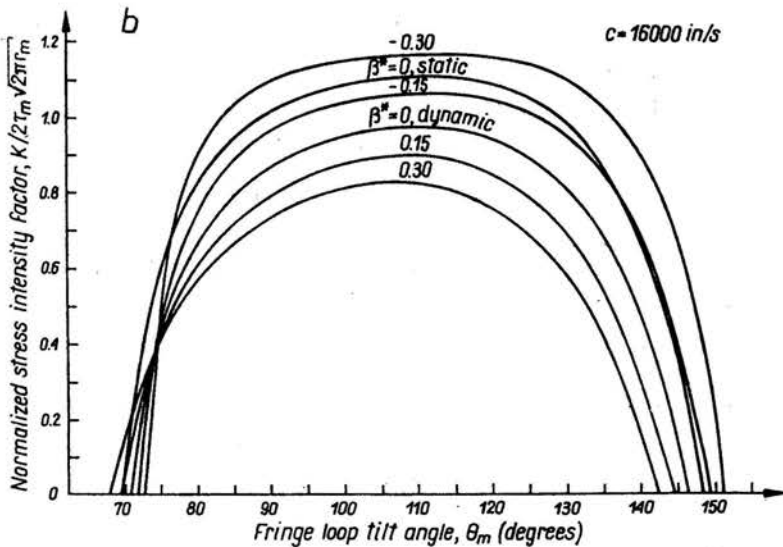
Fig. 3. Stress intensity factor K vs fringe loop tilt angle θ_m relationship for varying β, a) static case, b) high velocity running crack.
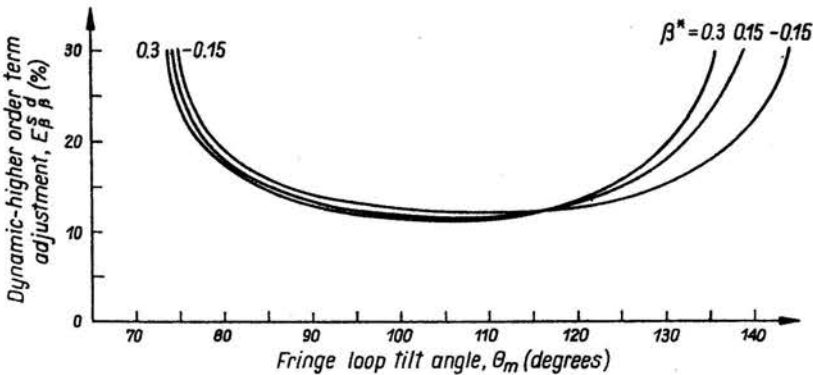
Fig. 4. Adjustment (relative error) $E_{\beta\beta}^{sd} \cdot 100\%$ associated with static 3-parameter method $\rightarrow$ dynamic 3-parameter method.

if one employs the static two-parameter method where $\beta = 0$ rather than the dynamic three-parameter method for the determination of K. Again, the minimum error due to velocity effects (in the case $\beta = 0$, $c = 16000''/s$) is about 11%; however, increasing positive β-values enlarge this minimum error whereas decreasing negative β^*-values in the range $0 > \beta^* > -0.4 \left(\beta^* = \beta \dfrac{r}{r_s} \right)$ lower the minimum error. The adjustment curves for negative β^*-values of magnitude around -0.4 are very complicated because of the presence of the strong singularity in the $\alpha^* - \beta^*$-plane [5].

The fundamental relation (18) may be combined with the stress-law

$$(19) \qquad\qquad \tau_m = \frac{N f_\sigma}{2h}$$
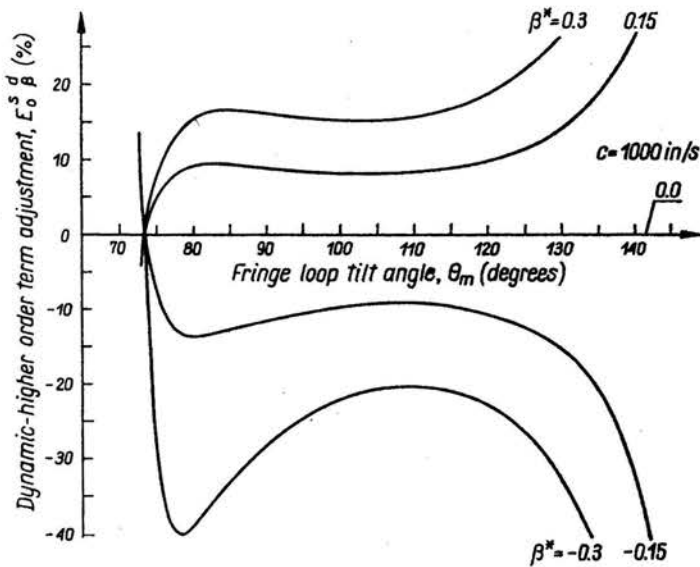
FIG. 5. Adjustment (relative error) $E_{0\beta}^{sd} \cdot 100\%$ associated with static 2-parameter method → dynamic 3-parameter method.

to yield a relation between K and the fringe order N:

$$(20) \qquad \frac{Kh}{Nf_\sigma} = H(\theta_m, r_m; \beta),$$

where f_σ is the stress-optical coefficient in terms of fringe order and h is the specimen thickness.

Equating a similar expression as Eq. (20) for two indenpendent loops yields

$$(21) \qquad \frac{N_2}{N_1} \frac{H(\theta_{m2}, r_{m2}, \beta)}{H(\theta_{m1}, r_{m1}, \beta)} = \frac{N_2}{N_1} \frac{G_1}{G_2} \sqrt{\frac{1+g_1^2}{1+g_2^2}} = \sqrt{\frac{r_{m1}}{r_{m2}}} \equiv \xi$$

provided the value of K is independent of the loop size ($K_1 = K_2$).

The values of the function H differ for different order fringe loops. This difference, however, is very small whenever adjacent loops in the range of $90° < \theta_m < 120°$ are selected. Thus, the parametric expression

$$(22) \qquad \xi = \frac{N_2}{N_1}(1+\delta)$$

enters the cubic equation (15). Because δ can be evaluated from the measurements of r_{mj} and the fringe orders N_j, ξ is a function of the ratio of the two loop orders and the apogee distances r_{mj}.

The value of K obtained depends on the fringe loop combination, i.e. a transition from one fringe loop to another gives a different K-value. The influence of the finite specimen boundaries on the loop shape and thus on the determination of K becomes larger for larger loops. The use of large isochromatic lobes which are more influenced by the β-term leads to an appreciable overestimation (underestimation) of the stress intensity factor
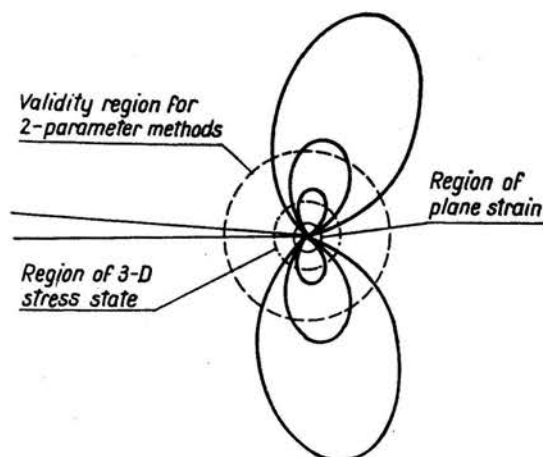
FIG. 6. The state of stress around a crack tip and the relative position of isochromatic fringe loops.

when the β-term has a negative (positive) sign. When dealing with loop combinations, where one loop is in the plane-strain region and the other loop extends into the plane-stress region, unreliable K-values may be obtained. The region of uncertain stress state is an annular zone around the crack tip whose mean radius is comparable to the plate thickness. Large scale loops are associated with plane stress strain conditions (Fig. 6). This effect can be accounted for by defining a coefficient $\bar{\varkappa}$ which characterizes the degree of transition from one state of stress to the other:

$$(23) \qquad \frac{K_1}{K_2} = 1 + \bar{\varkappa},$$

where K_1 and K_2 are associated with the large and small loop apogees, respectively.

Eqations (20), (2) and (23) may be combined to give

$$(24) \qquad \xi = \frac{N_2}{N_1}(1+\delta)(1+\bar{\varkappa}).$$

Is should be noted that $\varkappa$ changes with the relative size of the fringe loops, i.e. it is a function of the difference of fringe loop orders $N_2 - N_1$. The value of $\varkappa$ increases when $N_2 - N_1$ increases.

Appendix

The symbol $(\ )^{\cdot} \equiv \partial(\ )/\partial\theta$ is employed for the derivative with respect to the angle. Using the relations $(j = 1, 2)$,

$$(A.1) \qquad \gamma_j = \sqrt[4]{1 - (c/c_j)^2 \sin^2\theta},$$

$$(A.2) \qquad \dot{\gamma}_j = -\frac{1}{4}\left(\frac{c}{c_j}\right)^2 \frac{\sin 2\theta}{(1-(c/c_j)^2\sin^2\theta)^{3/4}},$$

(A.3)
$$C_s^j = \frac{1}{\gamma_j} \sin \frac{\theta_j}{2},$$

(A.4)
$$C_c^j = \frac{1}{\gamma_j} \cos \frac{\theta_j}{2},$$

(A.5)
$$D_s^j \equiv \frac{\partial}{\partial \theta} C_s^j = \frac{1}{2\gamma_j^5} \left\{ -r_j \cos \frac{\theta_j}{2} + \frac{1}{2} \left(\frac{c}{c_j} \right)^2 \sin \frac{\theta_j}{2} \sin 2\theta \right\},$$

(A.6)
$$D_c^j \equiv \frac{\partial}{\partial \theta} C_c^j = \frac{1}{2\gamma_j^5} \left\{ -r_j \sin \frac{\theta_j}{2} + \frac{1}{2} \left(\frac{c}{c_j} \right)^2 \cos \frac{\theta_j}{2} \sin 2\theta \right\}.$$

The functions F_j, G_j, and $\dot{g}_j = \dot{G}_j/\dot{F}_j$ have the form

$$F_j = F_{0j} + \beta \frac{r_{mj}}{a} F_{1j},$$

$$G_j = F_{0j} + \beta \frac{r_{mj}}{a} G_{1j},$$

(A.7)
$$\begin{aligned}
&F_{0j} = \Omega C_{cj}^2 - (1+r_1^2)C_{cj}^1, &&G_{0j} = 2r_1(C_{sj}^1 - C_{sj}^2), \\
&F_{1j} = \Omega C_{cj}^2 \gamma_{2j}^2 - (1+r_1^2)C_{cj}^1 \gamma_{1j}^2, &&G_{1j} = 2r_1(C_{sj}^2 \gamma_2^2 - C_{sj}^1 \gamma_1^2), \\
&\dot{F}_{0j} = \Omega D_{cj}^2 - (1+r_1^2)D_{cj}^1, &&\dot{G}_{0j} = 2r_1(D_{sj}^1 - D_{sj}^2), \\
&\dot{F}_{1j} = \Omega(D_{cj}^2 \gamma_{2j}^2 + C_{cj}^2 2\gamma_{2j}\dot{\gamma}_{2j}) - (1+r_1^2)(D_{cj}^1 \gamma_{1j}^2 + C_{cj}^1 2\gamma_{1j}\dot{\gamma}_{1j}), \\
&\dot{G}_{1j} = 2\gamma_1(D_{sj}^2 \gamma_{2j}^2 + C_{sj}^2 2\gamma_{2j}\dot{\gamma}_{2j} - D_{sj}^1 \gamma_{1j}^2 - C_{sj}^1 2\gamma_{1j}\dot{\gamma}_{1j}).
\end{aligned}$$

The coefficients of the cubic equation (15) are

(A.8)
$$\begin{aligned}
&\lambda_1 = T_{12}\dot{F}_{01}, &&\lambda_5 = T_{32}\dot{F}_{01}, &&\lambda_9 = T_{11}\dot{F}_{12}, \\
&\lambda_2 = T_{22}\dot{F}_{01}, &&\lambda_6 = T_{32}\dot{F}_{11}, &&\lambda_{10} = T_{21}\dot{F}_{12}, \\
&\lambda_3 = T_{12}\dot{F}_{11}, &&\lambda_7 = T_{11}\dot{F}_{02}, &&\lambda_{11} = T_{13}\dot{F}_{02}, \\
&\lambda_4 = T_{22}\dot{F}_{11}, &&\lambda_8 = T_{21}\dot{F}_{02}, &&\lambda_{12} = T_{31}\dot{F}_{12},
\end{aligned}$$

where

(A.9)
$$\begin{aligned}
T_{1j} &= F_{0j}\dot{F}_{0j} + G_{0j}\dot{G}_{0j}, \\
T_{2j} &= (F_{1j}F_{0j} + G_{1j}G_{0j})^{\cdot} \quad (j = 1, 2), \\
T_{3j} &= F_{1j}\dot{F}_{1j} + G_{1j}\dot{G}_{1j}.
\end{aligned}$$

The expressions for G, F, $\dot{G}$, $\dot{F}$, and g which appear in Eq. (17) are identical to the expressions (A-7) with the index j omitted.

Acknowledgement

References

1. G. R. IRWIN, Discussion to the paper by A. A. Wells and D. Post, (Proc. of SESA, 16, 96–92, 1958), Proc. of SESA, **16**, 93–96, 1958.
2. W. B. BRADLEY and W. B. KOBAYASHI, *An investigation of propagating cracks by dynamic photoelasticity*, Exp. Mech., 10, 3, 106–113, 1970.
3. J. M. ETHERIDGE et al., *A new method of determining the stress intensity factor K from isochromatic fringe loops*, Eng. Fract. Mechanics, **10**, 81–93, 1978.
4. J. M. ETHERIDGE and J. W. DALLY, *A three-parameter method for detemining stress intensity factors from isochromatic fringe loops*, J. Strain Analysis, **13**, 91–94, 1978.
5. H. P. ROSSMANITH and G. R. IRWIN, *Analysis of dynamic isochromatic crack-tip stress patterns*, University of Maryland Report 1978/79.
6. G. R. IRWIN, *Relatively unexplored aspects of fracture mechanics*, Univ. of Illinois, T. and A. M. Report 240, Feb. 1963, and Constant Speed Semi-infinite Crack, Lehigh Univ. Lecture Notes, 1968.

II. INSTITUT FÜR MECHANIK
TECHNISCHE UNIVERSITÄT WIENA, AUSTRIA.